PAPER • **OPEN ACCESS**

Complex dam break simulation using the 2-D depth-averaged SPH flow model: a validation for tsunami application

To cite this article: Muhammad Hafiz Aslami *et al* 2023 *IOP Conf. Ser.: Earth Environ. Sci.* **1169** 012026

Complex dam break simulation using the 2-D depth-averaged SPH flow model: a validation for tsunami application

Muhammad Hafiz Aslami[a], Benedict D. Rogers[b], Peter K. Stansby[b], Andrea Bottacin-Busolin[c]

[a]Civil Engineering Study Program, faculty of Engineering, Bina Nusantara University Jakarta, Indonesia
[b]Department of Mechanical, Aerospace and Civil Engineering, University of Manchester Manchester, UK
[c]Department of Industrial Engineering, University of Padua Padova, Veneto, Italy

E-mail: muhammad.hafiz004@binus.ac.id

Abstract. Dam break flow has a similar characteristic to the tsunami surge after the breaking wave. Therefore, it is often used in laboratory-scale experiments to study tsunamis and can be used as a benchmark for validating a numerical model. This paper presents a simulation of a complex dam break flow to validate the two-dimensional (2-D) depth-averaged Smoothed Particle Hydrodynamics (SPH) flow model which involves a non-submersible obstacle in the domain. The method can also be referred to as shallow-water equations SPH (SWE-SPH). With SPH, the wetting and drying interfaces are automatically solved without any additional trick or handling. Therefore, a dry bed dam break is specifically tested here. The numerical results are validated using experimental data from the literature. The model shows the ability to reproduce the flow fields, shocks, vortices and flow region transitions with reasonable accuracy compared to the experimental data, despite the vertical averaging process in the formulation. This model can be a robust tool for predicting the hazards caused by extreme floodings, such as dam breaks, flash floods and tsunamis in development planning.

1. Introduction

The dam break flow at the laboratory scale has been a widely used test case to validate a numerical model [1, 2, 3, 4, 5]. The dam breaking process is usually simplified as an upward sliding gate or a rotatable hinged gate, either a rigid or flexible gate. Any sudden flow generation method will generate a similar water flow characteristic, i.e. rapidly varying and supercritical flow which can be violent and destructive. This type of flow can represent water-related natural disasters such as flash floods, tsunamis and obviously dam breaks.

Many numerical models used a depth-averaged approach, instead of a full three-dimensional (3-D) model, to simulate floodings, including tsunamis, because of a much larger horizontal domain size compared to the water depth [6, 7, 8, 9]. In this case, the 3-D models become not practical in terms of computational cost. The numerical schemes implemented are usually mesh- or grid-based methods which have robust, accurate and are computationally fast. However, special treatments are required when dealing with wet-dry interfaces. The smoothed particle

hydrodynamics (SPH) version of the depth-averaged flow solver can address this problem automatically due to its Lagrangian nature.

SPH was originally developed for non-axisymmetric astrophysics simulations [10, 11], but in the last 20 years it has been used in solving a wide range of engineering applications. The first extension to free-surface flows was proposed by Monaghan [12]. Since then, with the recent advancements in the underlying theory and hardware acceleration utilising the Graphics Processing Unit (GPU) technology, the SPH method has become increasingly robust, accurate and widely used throughout many engineering fields [13, 14].

The shallow-water equations (SWEs) are a well-known set of equations to represent depth-averaged flow in large horizontal domains. The first attempts to solve the SWEs using SPH were achieved by Ata and Soulaïmani [15] and Rodriguez-Paz and Bonet [16]. Further advancements were then developed by different researchers [17, 3, 18, 19, 20, 21]. A similar level of accuracy was successfully achieved compared to the conventional methods and the computational cost can be reduced by means of hardware acceleration and parallelisation techniques.

A parallelised SWE-SPH model has been developed here by converting the full 3-D Navier-Stokes SPH software called DualSPHysics [14]. DualSPHysics is free and open-source software developed for fluid simulation and multi-physics. The highly efficient and parallelised nature of the software can be utilised for its depth-averaged version. The SWE-SPH formulation is provided in the following section, followed by the model validation by comparing with the complex dam break experiment conducted by Aureli *et al* [1].

2. Shallow-water equations (SWEs)

The SWEs are derived by depth-averaging the 3-D Navier–Stokes equations. This approach assumes that the vertical component of velocity is negligible whilst its horizontal component throughout the depth of the water is invariant, hence, the vertical pressure profile is hydrostatic. This method is more applicable for cases where the horizontal length scale is much greater than the vertical length scale.

The governing equations for depth-integrated shallow water flow in Lagrangian form are written as

$$\frac{\mathrm{d}d}{\mathrm{d}t} = -\nabla \cdot (d\boldsymbol{v}) \tag{1}$$

$$\frac{\mathrm{d}\boldsymbol{v}}{\mathrm{d}t} = -g\nabla d - g\nabla b + \boldsymbol{S}_f \tag{2}$$

where d represents the water depth, $\boldsymbol{v} = (v_x, v_y)$ is the depth-averaged velocity vector in horizontal coordinates, g is the gravitational acceleration, b represents the bed elevation and $\boldsymbol{S}_f$ is the bed friction source term.

Defining the density ρ as the amount of fluid mass per unit area in a 2-D horizontal domain, Equations (1) and (2) above are the same as the Euler equations with additional source terms. The density ρ is a standard variable used in any 3-D flow model, therefore, modifying the existing software such as DualSPHysics becomes undemanding.

Assuming that the fluid is incompressible, the density ρ and water depth d are related according to the following equation

$$\rho = \rho_w d \tag{3}$$

where ρ_w is the actual density (1000 kg/m^3 for water). By substituting Equation (3) into (1) and (2), the SWEs can then be written as

$$\frac{\mathrm{d}\rho}{\mathrm{d}t} = -\nabla \cdot (\rho\boldsymbol{v}) \tag{4}$$

$$\frac{\mathrm{d}\boldsymbol{v}}{\mathrm{d}t} = -\frac{g}{\rho_w}\nabla\rho - g\nabla b + \boldsymbol{S}_f \tag{5}$$

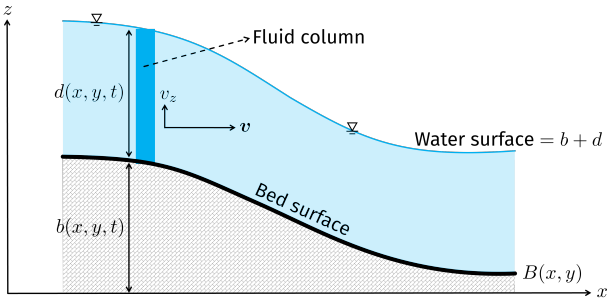

Figure 1. Illustration of a fluid particle as a column

3. Depth-averaged SPH formulation with variable resolution

The SWE-SPH formulation was derived from the variational approach for SPH [22] with variable smoothing length [23]. The depth-averaged version was developed later by Rodriguez-Paz and Bonet [16]. The detailed derivation is available in a paper written by Vacondio *et al* [17]. The final version of the equations are presented in this paper.

3.1. Momentum equation

In the depth-averaged representation of the fluid, an SPH particle becomes an SPH column of fluid. Figure 1 shows the particle representation of fluid in the computation domain. In a 2-D Cartesian coordinate system, the bathymetry data, denoted by $B(x, y)$ in 2-D horizontal coordinates, is fixed in time. A 2-D Cartesian coordinate system is used for the hydrodynamics model. Above the bed surface, the fluid is discretised as a set of Lagrangian particles each representing a column of water. Each fluid particle possesses properties including mass m which is constant in time, bed elevation b, depth d, position $\boldsymbol{x} = (x, y)$ and depth-averaged velocity $\boldsymbol{v} = (v_x, v_y)$. Using the variational formulation of Rodriguez-Paz and Bonet [16], the acceleration of the i-th fluid particle $\dfrac{\mathrm{d}\boldsymbol{v}_i}{\mathrm{d}t}$ including dissipative terms is given by:

$$\frac{\mathrm{d}\boldsymbol{v}_i}{\mathrm{d}t} = -\boldsymbol{t}_i - \frac{g + \boldsymbol{v}_i \cdot \boldsymbol{k}_i \boldsymbol{v}_i - \boldsymbol{t}_i \cdot \nabla b_i}{1 + \nabla b_i \cdot \nabla b_i} \nabla b_i + \boldsymbol{S}_{f,i} \tag{6}$$

where $\boldsymbol{t}_i = \boldsymbol{T}_i / m_i$,

$$\boldsymbol{T}_i = \sum_{j=1}^{N} m_i m_j \frac{g}{2\rho_w} \left(\frac{1}{\alpha_j} \nabla W_j(\boldsymbol{x}_i, h_j) - \frac{1}{\alpha_i} \nabla W_i(\boldsymbol{x}_j, h_i) \right) \tag{7}$$

and

$$\alpha_i = -\frac{1}{\rho_i D_m} \sum_j m_j r_{ij} \frac{\mathrm{d}W_{ij}}{\mathrm{d}r_{ij}} \tag{8}$$

The subscript j denotes the neighbour particles, N is the number of neighbours around particle i, α_i is the correction factor to account for the variable smoothing length, r_{ij} is the distance between particle i and j, D_m is the dimension (1 for one-dimensional (1-D) domain and 2 for 2-D), ρ_i is the 2-D density, W_{ij} is the smoothing kernel, $\nabla W_i(\boldsymbol{x}_j, h_i)$ is the kernel gradient of W with respect to the position of particle i and h_i is the smoothing length of the i-th particle. The fifth-order Wendland kernel [24] is used in this study.

3.1.1. Stabilisation term The SPH stabilisation technique based on the Lax-Friedrichs flux formulation proposed by Ata and Soulaïmani [15] is used here to avoid numerical oscillations.With this technique, no tuning parameters are needed as is in the artificial viscosity formulation by Monaghan [25]. The additional numerical viscosity term, Π_{ij}, can be included in (7) to preserve the stability as:

$$\boldsymbol{T}_i = \sum_j m_i m_j \left[\left(\frac{g}{2\rho_w} \frac{1}{\alpha_j} + \frac{\Pi_{ij}}{2} \right) \nabla W_j(\boldsymbol{x}_i, h_j) - \left(\frac{g}{2\rho_w} \frac{1}{\alpha_i} + \frac{\Pi_{ij}}{2} \right) \nabla W_i(\boldsymbol{x}_j, h_i) \right] \tag{9}$$

The Π_{ij} is calculated using the following equation

$$\Pi_{ij} = -\frac{\bar{c}_{ij} \boldsymbol{v}_{ij} \cdot \boldsymbol{x}_{ij}}{\bar{\rho}_{ij} \sqrt{|\boldsymbol{x}_{ij}|^2 + \eta^2}} \tag{10}$$

where $c = \sqrt{gd}$ is the wave speed, $\bar{\bullet}_{ij} = 0.5(\bullet_i + \bullet_j)$ and $\eta = 0.1\bar{h}_{ij}$ is a small denominator to prevent division by zero.

3.1.2. Bed gradient and bed friction source term A set of fixed particles are introduced at the beginning of the simulation to represent the irregular bathymetry or bed profile. These bed particles are distributed in a uniform grid as described by Vacondio *et al* [18]. These bed particles possess both the bed surface elevation and Manning coefficient which are then used to approximate the bed gradient ∇b_i using the SPH approximation combined with the correction method of Bonet and Lok [22], and to interpolate the bed curvature tensor $\boldsymbol{k}_i = \nabla(\nabla b_i)$ using the integral approximation by Cleary and Monaghan [26, 27]. The bed particles are also used to interpolate the Manning coefficient n_i using the scatter SPH summation with a Shepard filter [28]. This is then used to estimate the bed friction source term $\boldsymbol{S}_{f,i}$ below:

$$\boldsymbol{S}_{f,i} = -g n_i^2 \frac{|\boldsymbol{v}_i| \boldsymbol{v}_i}{d_i^{4/3}} \tag{11}$$

3.2. Continuity equation

The mass of each fluid particle remains constant during a simulation. Therefore, to allow the change of a particle's water depth, the volume and hence smoothing length of the particle also change. In variable-h SPH form, the density of the i-th particle is approximated as follows:

$$\rho_i = \sum_j m_j W_i(\boldsymbol{x}_j, h_i) \tag{12}$$

The density ρ (or depth d) may vary significantly during a simulation, especially when a particle moves into and out of shallow water when the fluid is expanding or compressing. To maintain a constant accuracy, an approximately constant number of neighbouring particles must be maintained by adjusting the smoothing length [29] according to:

$$h_i = h_{i,0} \left(\frac{\rho_{i,0}}{\rho_i} \right)^{1/D_m} \tag{13}$$

where $\rho_{i,0}$ and $h_{i,0}$ are the density and smoothing length of the i-th particle at the beginning of simulation. Equations (12) and (13) are implicit requiring an iterative solution such as the Newton-Raphson method described in [16]. Once the converged values of ρ_i and h_i are found, the water depth is updated as $d_i = \rho_i/\rho_w$. Since the fluid is assumed to be incompressible, the area of particle V_i (equivalent to volume in 3-D SPH) is also changed following $V_i = m_i/\rho_i$ to keep the volume of fluid column constant.

3.3. Solid wall boundary conditions

The solid wall is represented by a set of particles called wall boundary particles (WBPs) distributed in a uniform grid filling the wall shape. The particles have the same properties as the fluid including mass m, density ρ and depth d. The WBPs are considered as neighbours when computing the summations in the fluid momentum equation (6) and continuity equation (12). To impose the no-slip boundary condition, the density and velocity of the i-th WBP are extrapolated from the fluid body using SPH interpolation as follows:

$$\rho_i = \sum_{j \in \text{fluid}} \rho_j \overline{W}_i(\boldsymbol{x}_j, h_j) V_j \tag{14}$$

$$\boldsymbol{v}_i = -\sum_{j \in \text{fluid}} \boldsymbol{v}_j \overline{W}_i(\boldsymbol{x}_j, h_j) V_j \tag{15}$$

where $\overline{W}_i(\boldsymbol{x}_j, h_j) = \dfrac{W_i(\boldsymbol{x}_j, h_j)}{\sum_{j \in \text{fluid}} W_i(\boldsymbol{x}_j, h_j)}$ is the corrected kernel using the Shepard filter [28] and V_j is the particle's area. After the density of all WBPs has been calculated, we can then assign their depth $d_i = \rho_i / \rho_w$ and mass $m_i = \rho_i / V_i$. In Equations (14) and (15), the smoothing length of the neighbouring particles h_j is used with the so-called scatter SPH formulation. The scatter formulation is used to ensure that each WBP found in the fluid's kernel radius has the required values for the summation. Boundary particles can be placed in a fixed position or moved according to predefined motion. This boundary treatment therefore functions in a similar manner to the dummy particles method [30] retaining the advantages such as an easy set up, efficient and robust for complex wall geometries.

3.4. Time integration scheme

The explicit second-order symplectic scheme is used in this paper, which involves predictor and corrector steps, to integrate (6) in time. The predictor stage is used to evaluate the evolution in the middle of the time step:

$$\boldsymbol{v}_i^{n+\frac{1}{2}} = \boldsymbol{v}_i^n + \frac{\Delta t}{2} \left(\frac{\mathrm{d}\boldsymbol{v}}{\mathrm{d}t} \right)_i^n \tag{16}$$

$$\boldsymbol{x}_i^{n+\frac{1}{2}} = \boldsymbol{x}_i^n + \frac{\Delta t}{2} \boldsymbol{v}_i^n \tag{17}$$

where n denotes the time step and Δt is the time step interval. The force computed at the middle time step is then used to evaluate the value at the end of the time step, which is referred to as the corrector stage:

$$\boldsymbol{v}_i^{n+1} = \boldsymbol{v}_i^n + \Delta t \left(\frac{\mathrm{d}\boldsymbol{v}}{\mathrm{d}t} \right)_i^{n+\frac{1}{2}} \tag{18}$$

$$\boldsymbol{x}_i^{n+1} = \boldsymbol{x}_i^n + \Delta t \frac{\left(\boldsymbol{v}_i^{n+1} + \boldsymbol{v}_i^n \right)}{2} \tag{19}$$

We use the variable time step Δt in the model. For an explicit integration scheme, the time step must satisfy the Courant-Friedrichs-Lewy (CFL) condition [31]

$$\begin{aligned} \Delta t &= C_{CFL} \ \min\left(\Delta t_v, \Delta t_a\right), \text{where} \\ \Delta t_v &= \min_{i=1}^{N_f} \left(\frac{h_i}{c_i + |\boldsymbol{v}_i|} \right) \text{and} \\ \Delta t_a &= \min_{i=1}^{N_f} \left(\sqrt{\frac{h_i}{\left| \frac{\mathrm{d}\boldsymbol{v}_i}{\mathrm{d}t} \right|}} \right) \end{aligned} \tag{20}$$

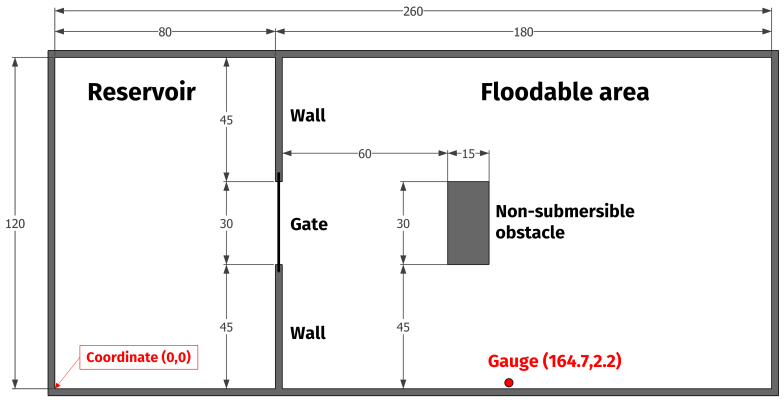

Figure 2. The dimension (in cm) of the experimental facility in plan view

C_{CFL} is the Courant number whose value is 0.2 in this paper and N_f is the number of fluid particles. Δt_v and Δt_a are the time step limit based on fluid velocity and acceleration respectively.

4. Results

4.1. Simulation configuration

The simulation configuration is set to reproduce the experimental dam break flow carried out at the Hydraulic Laboratory of Parma University by Aureli *et al* [1], as illustrated in Figure 2. A rectangular tank is divided into two sections functioning as a reservoir and a floodable area. The tank is equipped with a sluice gate powered by a pneumatic piston at the middle of the dividing wall. The sudden removal of the gate will initiate the water flow into the initially dry floodable area. A non-submersible and fixed rectangular prism is located in the middle of the dry tank to achieve a strong perturbation of the flooding dynamics. Point measurement of a water depth time series by means of an ultrasonic distance meter is recorded at position $x = 1.647$ m and $y = 0.022$ m, with which the numerical results are compared.

4.2. Numerical results

The numerical simulation domain was initially discretised into particles by means of a Cartesian grid arrangement. For this particular test case, the particle size was 5 mm giving 38,577 fluid particles, 12,262 wall boundary particles and 136,425 particles for bathymetry. The Manning coefficient for bed friction source term computation was set at 0.007 s $m^{-1/3}$ based on a calibration carried out by Aureli *et al* [1].

The comparison of experimental and numerical results of water depth is shown in Figure 3 where several snapshots at the different time frames from the plan view are presented. The first frame at $t = 0.4$ s shows the initial water flow after the gate release just before impacting the obstacle. A disagreement was observed here due to the 3-D effect of water falling at the breach site during the initial stage which cannot be represented correctly by the depth-averaged model. Besides, the gate removal time was not as spontaneous as assumed in the numerical model.

In the second frame ($t = 0.75$ s), a shock wave occurred due to the impact of the water with the obstacle. The model was able to reproduce the flow transition from supercritical to subcritical which generated a hydraulic jump. The chaotic characteristic shown in the experiment, which involved water-air interactions, seemed to be smoothed out in the numerical model due to the numerical dissipation and the incapability to capture the 3-D multi-phase effect. The sharpness of the shocks, however, may be increased by implementing any shock-

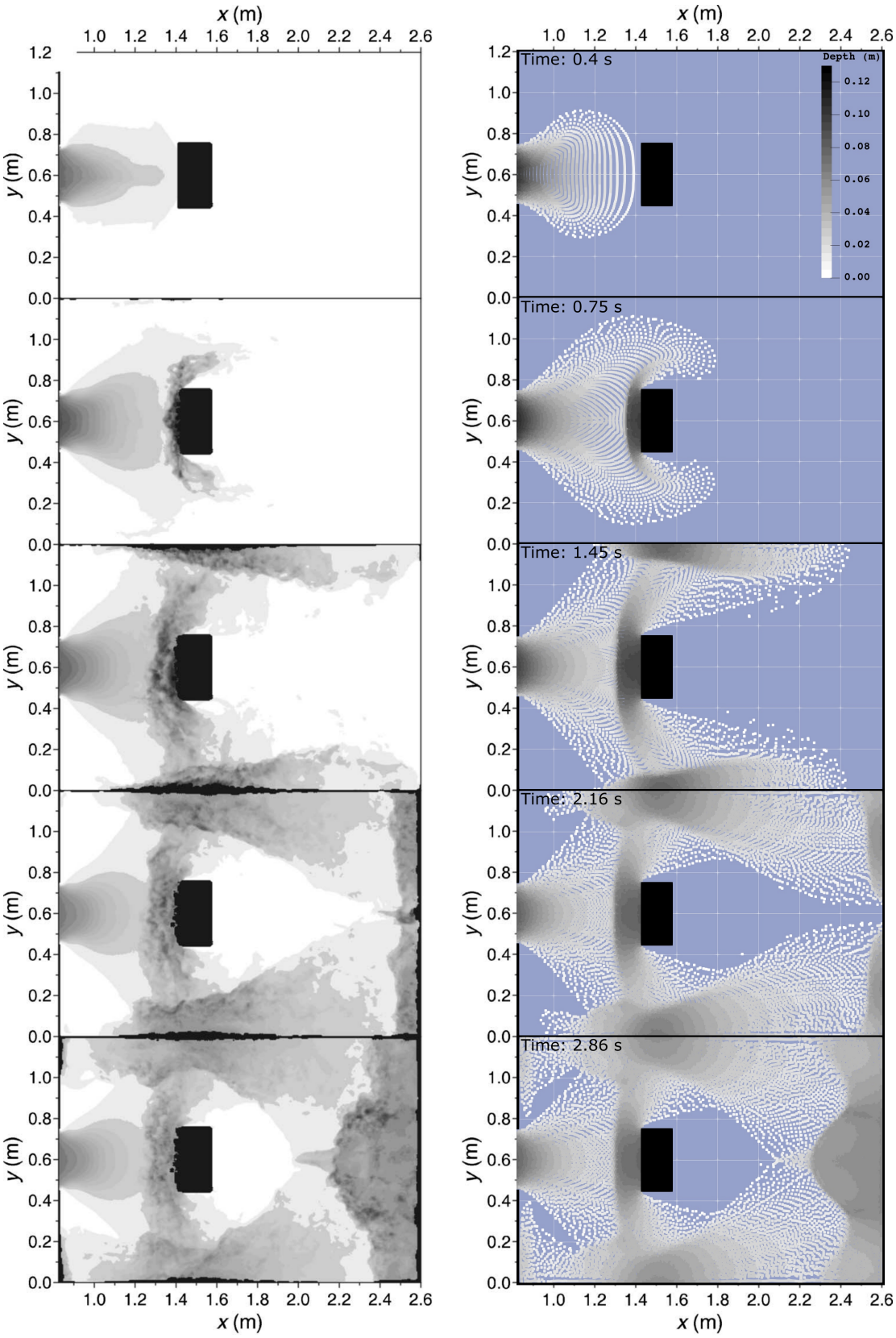

Figure 3. The plan view snapshots of experimental (left) [1] and SWE-SPH numerical (right) water depths at $t = 0.4$ s, $t = 0.75$ s, $t = 1.45$ s, $t = 2.16$ s and $t = 2.86$ s

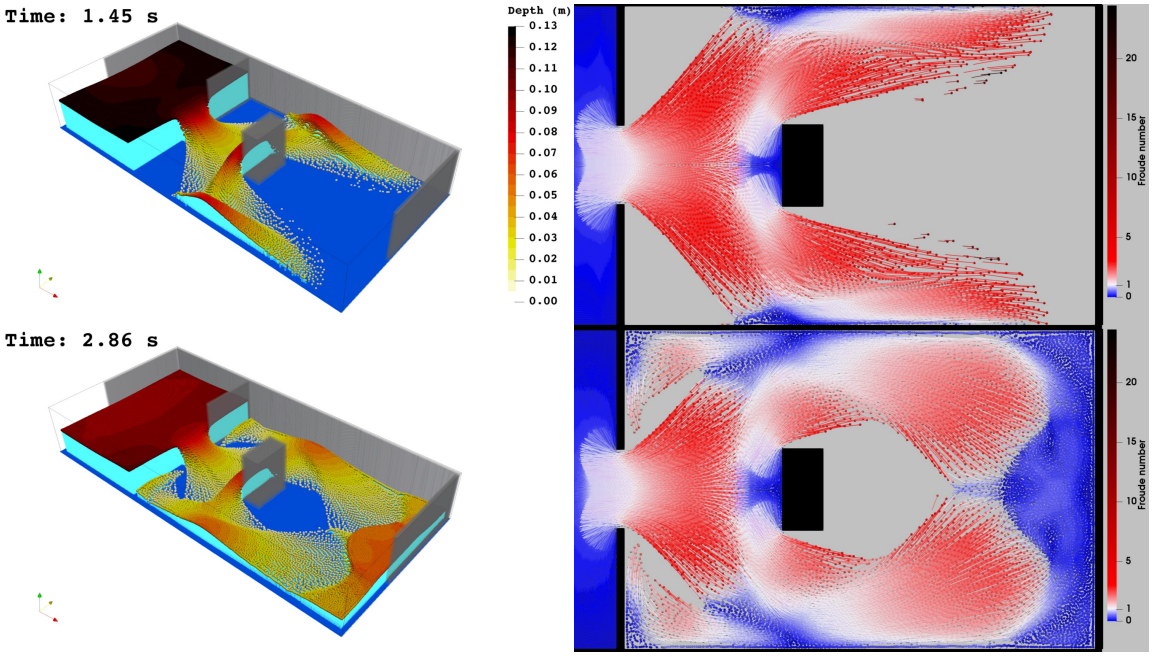

Figure 4. The 3-D (left) and velocity vectors (right) plots of the numerical results

capturing methods available or simply by using finer particle resolution with the expense of more computational effort. In the next frame ($t = 1.45$ s), the hydraulic jump near the obstacle was moving upstream whilst another two shock waves emerged due to the flow impact with the side walls. The following shocks were also clearly visible near the downstream wall at $t = 2.16$ s. Not long after, the reflected wave started to propagate upstream at $t = 2.86$ s. The SWE-SPH model successfully reproduced the general phenomenon of the complex dam break flow except at specific areas and times where a strong 3-D effect took place.

Another complexity reproduced by the numerical model was the vortices shown on the right-hand side in Figure 4. Each particle was plotted as an arrow whose length was linearly correlated with the velocity magnitude. The flow circulation was found at several locations near the wall. On the left-hand side, a 3-D plot is presented showing the water surface dynamics during simulation. The tank and obstacle were clipped off halfway along $y = 0.6$ m to give more visibility of the water flow. Several hydraulic jumps clearly present in the flow. If we look back to the velocity vector plot, the arrows were coloured based Froude number (Fr) from 0 (blue) to 25 (dark red) separated by $Fr = 1$ (white). From those coloured maps, we can clearly see the flow transitions from supercritical ($Fr > 1$) to subcritical ($Fr < 1$), which developed hydraulic jumps, and vice versa.

Figure 5 compares the water depth time series captured in the experiment by means of an ultrasonic transducer and the numerical result at the same position ($x = 1.647$ m and $y = 0.022$ m). The numerical result shows a good general agreement with the experimental data. The arrival time of the front surge was precisely predicted as well as the reflected wave at $t = 4.5$ s. However, the SWE-SPH model could not capture the first shock after the flow impact on the side wall. A 3-D model is suggested to reproduce this problem more accurately, especially using an SPH model which specialises in free surface hydrodynamics modelling.

To quantify the overall accuracy of the model, two statistical parameters are analysed,

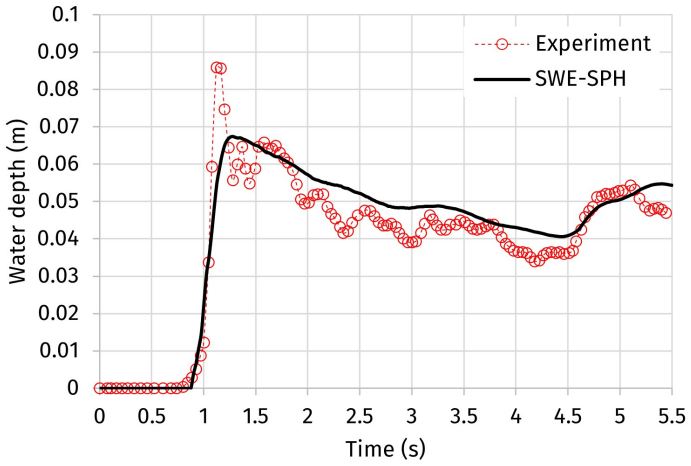

Figure 5. The water depth time series of experimental and numerical point measurements

amplitude A_s and phase P_s [32]:

$$A_s = \sqrt{\frac{\sum_{t=1}^{N_t} d_t^2}{\sum_{t=1}^{N_t} d_{t,exp}^2}} \quad \text{and} \tag{21}$$

$$P_s = \sqrt{\frac{\sum_{t=1}^{N_t} (d_t - d_{t,exp})^2}{\sum_{t=1}^{N_t} d_{t,exp}^2}} \tag{22}$$

where t is the time step, N_t is the total number of time series data, d_t is the numerical water depth at time t and $d_{t,exp}$ is the experimental depth. A perfect agreement gives $A_s = 1$ and $P_s = 0$. In this case, the data in Figure 5 gives $A_s = 1.076$ and $P_s = 0.142$ which is reasonably accurate for such complex flow.

5. Conclusion

A complex laboratory scale dam break simulation has been simulated using a depth-averaged SPH flow model and the results agreed well with the experimental measurement. The flow field characteristic was complex involving strong reflections, shocks, vortices, and flow regime transition. Despite the complexity, the SWE-SPH model accurately predicted the water flow. Quantification of the accuracy is calculated using two statistical parameters: amplitude $A_s = 1.076$ and phase $P_s = 0.142$. Perfect agreement would give 1 and 0, respectively, for both parameters.

The hydraulic jumps, however, seemed to be smoothed out due to the numerical dissipation. The additional shock-capturing method is desired to catch the shock better. Additionally, the complexity of the flow field in this work was mainly caused by the solid wall and obstacle configuration while the bed surface remained flat. Therefore, the effect of irregular bathymetry on wave dynamics was not examined. This will be kept for future work. As a final remark, the flow model has a high potential to be a robust tool to simulate tsunami floodings, which is essential in planning the infrastructure development in tsunami-prone areas, but further improvements are still needed for practical use in the actual case.

References

[1] Aureli F, Maranzoni A, Mignosa P and Ziveri C 2008 *Journal of hydraulic engineering (New York, N.Y.)* **134** 1089–1101 ISSN 0733-9429
[2] Aureli F, Maranzoni A, Mignosa P and Ziveri C 2011 *Experiments in Fluids* **50** 665–675 ISSN 07234864
[3] Vacondio R, Rogers B D, Stansby P K and Mignosa P 2013 *Advances in Water Resources* **58** 10–23 ISSN 03091708 URL http://dx.doi.org/10.1016/j.advwatres.2013.04.007
[4] Zhang Y and Lin P 2016 *Proceedings of the Institution of Civil Engineers: Water Management* **169** 260–274 ISSN 17517729
[5] Magdalena I, Hariz A, Farid M and Kusuma M S B 2021 *Results in Applied Mathematics* **12** 100193 ISSN 25900374 URL https://doi.org/10.1016/j.rinam.2021.100193
[6] Goto C, Ogawa Y, Shuto N and Imamura F 1997 *IUGG/IOC Time Project, IOC Manuals and Guides No. 35: Numerical Method of Tsunami Simulation with the Leap-Frog Scheme* (Paris: UNESCO)
[7] Wang X 2009 *USER MANUAL FOR COMCOT VERSION 1.7* (Cornell University) URL https://citeseerx.ist.psu.edu/viewdoc/download?doi=10.1.1.512.84&rep=rep1&type=pdf
[8] Titov V and González F 1997 *NOAA Tech. Memorandum ERL PMEL-112*
[9] Center H E 2021 HEC-RAS 2D Modeling User's Manual
[10] Gingold R A and Monaghan J J J 1977 *Monthly notices of the royal astronomical society* **181** 375–389 ISSN 1365-2966
[11] Lucy L B 1977 *The Astronomical Journal* **82** 1013 ISSN 00046256 (*Preprint* 9809069v1) URL http://adsabs.harvard.edu/cgi-bin/bib_query?1977AJ.....82.1013L
[12] Monaghan J J 1994 *Journal of Computational Physics* **110** 399–406 ISSN 00219991
[13] Violeau D and Rogers B D 2016 *Journal of Hydraulic Research* **54** 1–26 ISSN 00221686
[14] Domínguez J M, Fourtakas G, Altomare C, Canelas R B, Tafuni A, García-Feal O, Martínez-Estévez I, Mokos A, Vacondio R, Crespo A J C, Rogers B D, Stansby P K and Gómez-Gesteira M 2021 *Computational Particle Mechanics* ISSN 2196-4386 URL https://doi.org/10.1007/s40571-021-00404-2
[15] Ata R and Soulaïmani A 2005 *International Journal for Numerical Methods in Fluids* **47** 139–159 ISSN 02712091
[16] Rodriguez-Paz M and Bonet J 2005 A corrected smooth particle hydrodynamics formulation of the shallow-water equations *Computers and Structures* vol 83 pp 1396–1410 ISBN 1098-2426 ISSN 00457949
[17] Vacondio R, Rogers B D and Stansby P K 2012 *International Journal for Numerical Methods in Fluids* **69** 1377–1410 ISSN 02712091 (*Preprint* fld.1)
[18] Vacondio R, Rogers B D and Stansby P K 2011 *International Journal for Numerical Methods in Fluids* **69** 226–253 ISSN 02712091 (*Preprint* fld.1)
[19] Vacondio R, Rogers B D, Stansby P K and Mignosa P 2012 *Journal of Hydraulic Engineering* **138** 530–541 ISSN 0733-9429
[20] Wu Y, Tian L, Rubinato M, Gu S, Yu T, Xu Z, Cao P, Wang X and Zhao Q 2020 *Water (Switzerland)* **50** ISSN 20734441
[21] Xia X and Liang Q 2016 *Environmental Modelling and Software* **75** 28–43 ISSN 13648152 URL http://dx.doi.org/10.1016/j.envsoft.2015.10.002
[22] Bonet J and Lok T S 1999 *Computer Methods in Applied Mechanics and Engineering* ISSN 00457825
[23] Bonet J, Kulasegaram S, Rodriguez-Paz M X and Profit M 2004 *Computer Methods in Applied Mechanics and Engineering* ISSN 00457825
[24] Wendland H 1995 *Advances in computational Mathematics* **4** 389–396 ISSN 1019-7168
[25] Monaghan J J 1988 *Computer Physics Communications* **48** 89–96 ISSN 00104655 (*Preprint* arXiv:1007.4184v1)
[26] Cleary P W and Monaghan J J 1999 *Journal of Computational Physics* **148** 227–264 ISSN 00219991
[27] Monaghan J J 2005 *Reports on Progress in Physics* **68** 1703–1759 ISSN 00344885 (*Preprint* 0507472)
[28] Randles P W and Libersky L D 1996 *ELSEVIER Comput. Methods Appl. Mech. Engrg* **139** 375–408
[29] Benz W 1990 Smooth particle hydrodynamics: a review *The numerical modelling of nonlinear stellar pulsations* (Springer) pp 269–288
[30] Adami S, Hu X Y and Adams N A 2012 *Journal of Computational Physics* **231** 7057–7075 ISSN 00219991
[31] Toro E F 2001 *Shock-capturing methods for free-surface shallow flows* (John Wiley New York) ISBN 0471987662
[32] Gomez-Gesteira M, Rogers B D, Dalrymple R A and Crespo A J C 2010 *Journal of Hydraulic Research* **48** 000 ISSN 0022-1686 URL https://www.tandfonline.com/doi/full/10.1080/00221686.2010.9641242